

Article

Phenotypic and Biomechanical Characteristics of Human Fetal Neural Progenitor Cells Exposed to Pesticide Compounds

Marissa C. Sarsfield, Jennifer Vasu, Sabreen M. Abuoun, Nischal Allena and Chandrasekhar R. Kothapalli * 

Department of Chemical and Biomedical Engineering, 2121 Euclid Avenue, Cleveland State University, Cleveland, OH 44115, USA

* Correspondence: c.kothapalli@csuohio.edu; Tel.: +1-216-687-2562

Abstract: Various forms of pesticides have been reported to be among the environmental toxicants, which are detrimental to human health. The active ingredients of these formulations can enter the human body through air, food, or water. Epidemiological studies suggest that these compounds strongly affect the developing brain in fetal and infant stages due to their ability to breach the underdeveloped blood–brain barrier. Since neural progenitor stem cells (NPCs) in the developing brain are the most vulnerable to these compounds, the mechanisms by which NPCs experience toxicity upon exposure to these chemicals must be investigated. Here, we assessed the viability of human fetal NPCs in 2D cultures in the presence of the active ingredients of six widely used pesticides using Live/Dead[®] and Hoechst staining. The IC₅₀ values ranged from 4.1–201 μM. A significant drop in cell viability with increasing toxicant concentration ($p < 0.01$) was noted, with the order of toxicity being malathion < 4-aminopyridine < methoprene < prallethrin < temephos < pyriproxyfen. Changes in cellular biomechanical characteristics (Young's modulus, tether force, membrane tension, and tether radius) were quantified using atomic force microscopy, whereas cell migration was elucidated over 48 h using a customized wound-healing assay. The Young's modulus of fetal NPCs exposed to IC₅₀/2 doses of these compounds was reduced by 38–70% and that of those exposed to IC₅₀ doses was reduced by 71–80% ($p < 0.001$ vs. controls for both; $p < 0.01$ for IC₅₀ vs. IC₅₀/2 for each compound). Similar patterns were noted for tether forces and membrane tension in fetal NPCs. NPC migration was found to be compound type- and dose-dependent. These results attest to the significant detrimental effects of these compounds on various aspects of the human fetal NPC phenotype, and the utility of cell mechanics as a marker to assess developmental neurotoxicity.

Keywords: pesticides; fetal neural stem cells; cell mechanics; Young's modulus; tether forces; developmental neurotoxicity



Citation: Sarsfield, M.C.; Vasu, J.; Abuoun, S.M.; Allena, N.; Kothapalli, C.R. Phenotypic and Biomechanical Characteristics of Human Fetal Neural Progenitor Cells Exposed to Pesticide Compounds. *Biophysica* **2023**, *3*, 348–361. <https://doi.org/10.3390/biophysica3020023>

Academic Editor: Sapun Parekh

Received: 15 March 2023

Revised: 27 April 2023

Accepted: 12 May 2023

Published: 18 May 2023



Copyright: © 2023 by the authors. Licensee MDPI, Basel, Switzerland. This article is an open access article distributed under the terms and conditions of the Creative Commons Attribution (CC BY) license (<https://creativecommons.org/licenses/by/4.0/>).

1. Introduction

A broad family of pesticides (e.g., herbicides, insecticides, piscicides, fungicides, and disinfectants), synthetic or natural in origin, are being widely used worldwide for agricultural and household purposes. Global pesticide usage stands at around 3.5 million tons, [1] and its contributions to food security have been documented [2]. However, their storage and disposal, as well as their active ingredients and degraded byproducts, pose severe challenges to all living species [2–4]. Their bioaccumulation, persistence, inherent toxicity, and ability to infiltrate food chains and water resources have severe repercussions on human health, specifically on the endocrine and reproductive systems and fetal development [5–9]. Besides the active ingredients, a plethora of other compounds exist in these formulations, although their identities, compositions, and toxicological effects remain unknown [10].

Humans are exposed to pesticides either directly (e.g., occupation, agriculture, or domestic activities) or indirectly (e.g., air, water, or food), and these organic molecules, as well as their byproducts, can enter the physiological systems via dermal, oral, and respiratory tracks. Such exposure has been reported to affect human health (nervous system, skin and

eyes, endocrine system, hormonal pathways, and carcinogenicity) depending on the dose and exposure levels [11–14]. Some of these compounds were banned in the European Union, but they are still prevalent in many developing countries and the United States.

For instance, methoprene is a growth regulator insecticide that interferes with the life cycle of insects (e.g., house flies, mosquitoes, fire ants, and moths) by preventing maturation and reproduction [15,16]. It is typically sprayed on drinking and agricultural water sources, on domesticated animals for flea control, and as a food additive for cattle. Similarly to methoprene, pyriproxyfen is an insect growth regulator affecting young insects and their eggs (e.g., fleas, cockroaches, ticks, ants, carpet beetles, and mosquitoes) [17]. It is used inside homes and agricultural settings for flea and tick control of domesticated animals. Malathion is an organophosphate (OP) insecticide that is used in various agricultural and residential settings to control mosquitoes, fruit flies, and lice [18]. It works by inhibiting the cholinesterase enzyme that leads to continuous nervous firing, thereby preventing the insect from moving or breathing. Another OP insecticide, temephos, is typically applied to standing water (e.g., shallow ponds and lakes) to target aquatic larvae (e.g., mosquitoes and sandflies) [19]. Prallethrin is a synthetic pyrethroid insecticide used primarily to target ants, cockroaches, fleas, and ticks [20,21]. It can modify sodium channels to delay closure, causing repetitive nerve firing, and act on γ -Aminobutyric acid (GABA)-gated chloride channels resulting in seizures. Many food industries have received permission to add it to consumables at less than 1 ppm levels. Finally, 4-aminopyridine (4-AP) is used as a popular bird repellent (e.g., Avitrol) in agricultural fields, airports, and around livestock pens [22]. These six compounds are representative of many other pesticides used widely in several daily applications.

Numerous epidemiological studies link pesticide usage and exposure to neurodevelopmental defects in newborns and children [23–26]. These inferences were drawn from prospective and retrospective studies conducted in various countries across the globe involving cohorts of thousands of mother–child pairs, using levels measured from in utero, cord serum collected at birth, or postnatally. OP-based pesticides are among those widely studied in this regard, especially in developing countries, which have been shown to specifically target the vulnerable nervous system both in utero and in postnatal stages [27]. Neurodevelopmental defects linked to OP-based pesticides include abnormalities in neonatal reflexes, motor and sensory functions, neurobehavior, and psychomotor development index scores, as well as stunted head circumference, low IQ levels, attention-deficit hyperactivity disorder, and compromise in speech and cognitive skills [12]. Despite such population-level information, how these compounds induce biomechanical changes in human cells, especially in those derived from developmental stages, remains understudied. Such information is critical as biomechanical changes in cells could significantly affect their genotype and shape, as well as their functions, such as migration, differentiation, and mechanotransduction, during early developmental stages [28,29].

In this study, we used atomic force microscopy (AFM) and immunofluorescence assays to determine the effects of six representative insecticide compounds on a human fetal neural stem cell line (ReNcell VM NPCs). The NPCs were maintained in their undifferentiated, multipotent state throughout the study. The IC_{50} values of these six compounds were assessed in vitro, and their influence on the NPC phenotype, survival, and changes in biomechanical (Young's modulus, tether force, membrane tension, and tether radius) characteristics was quantified.

2. Materials & Methods

2.1. Materials

Dulbecco's Modified Eagle Medium (DMEM/F12), mouse-derived laminin, phosphate-buffered saline ($1 \times$ PBS), Accutase Enzyme cell detachment medium, Hoechst 33342 trihydrochloride trihydrate (10 mg/mL), and Nunclon™ Delta surface flat bottom 96-well plates were obtained from Thermo Fisher Scientific (Waltham, MA, USA). ReNcell NPC maintenance media (SCM005), culture-grade epidermal growth factor (EGF), fibroblast growth factor basic protein (bFGF), calcein-AM staining solution, and tissue culture grade

Penicillin/Streptomycin/Amphotericin B solution (100×) were obtained from EMD Millipore (MilliporeSigma, Burlington, MA, USA). 4-aminopyridine (4-AP), temephos (TE), malathion (MA), pyriproxyfen (PY), prallethrin (PR), methoprene (ME), dimethyl sulfoxide (DMSO), and acetone were obtained from Sigma Aldrich (St. Louis, MO, USA).

2.2. Cell Culture and Compound Concentrations

Human neural progenitor cells (ReNcell VM; SCC008; EMD Millipore) were cultured in an undifferentiated state in ReNcell maintenance medium supplemented with 20 ng/mL each of bFGF and EGF and 1% penicillin/streptomycin on 20 µL/mL laminin-coated flasks. These cells are *v-myc* immortalized and derived from ventral mesencephalon tissue dissections of a ten-week-old fetus [30]. Stock solutions of 4-AP, temephos, and malathion were prepared in filtered DMSO at 0.3 M concentrations, while pyriproxyfen, prallethrin, and methoprene stock solutions at 0.3 M were prepared in filtered acetone. The working concentrations of the compounds (10 pM, 100 pM, 1 nM, 10 nM, 100 nM, 1 µM, 10 µM, 100 µM, 1 mM, and 10 mM) were prepared by serial dilution of stock solutions in a culture medium and stored at 4 °C till usage.

2.3. Cell Viability Assay

ReNcells were cultured at a density of 10,000 cells/well on laminin-coated 96-well plates for 24 h and exposed to various concentrations of individual compounds for 24 h ($n = 4$ wells/concentration/compound). Control cultures that did not receive the compounds received DMSO or acetone at stock solution equivalent concentrations. In our pilot studies, such concentrations (0.1%) of DMSO or acetone exhibited no detectable adverse effect on ReNcells. Cell survival was assessed using calcein AM (0.25 µM) staining. Images were obtained using an automated fluorescent microscope (S+ scanner, Samsung Electro-Mechanics, Co., SEMCO, Suwon-si, Republic of Korea) with an excitation (Ex) set at 500–560 nm and emission (Em) set at 580–660 nm filter.

2.4. DNA Content Assay

The assay was performed with an initial seeding density of 10,000 cells/well on laminin-coated 96-well plates ($n = 4$ wells/concentration/compound). Hoechst 33342 (15 µM; Ex—352 nm/Em—416 nm) in 1× PBS (pH ~7.2) was used for the DNA content assay. After exposure to the individual compounds for 24 h, the media was replaced, and cells were incubated with Hoechst 33342 for 30 min to assess changes in nucleic DNA content. Control cultures that did not receive the compounds received DMSO or acetone at stock solution equivalent concentrations. An S+ scanner with a 4× objective and blue fluorescence filter (Semrock, DAPI-5060C-000; Ex: 340–405 nm/Em: 410–481 nm filter) was used to image the nuclei in each well. At least $n = 4$ wells/concentration/compound was tested.

2.5. Cell Survival Quantification

The fluorescence intensities of the images obtained from the cell viability assay and DNA content assay were quantified using NIH ImageJ. The images were converted to a 16-bit binary format (grey scale), the background was subtracted, and thresholding was applied uniformly to convert the images to black and white. The intensity was measured based on the number of white pixels. The intensity of each image was normalized to that in control wells. To determine the effect of the toxicant on the cells, dose–response curves from each assay were generated for each compound. The average normalized survival at each concentration was plotted against the logarithm of the compound concentration. From this, a sigmoidal dose–response curve was fitted using GraphPad Prism software (Boston, MA, USA) to determine the IC₅₀ values of each compound. The four-parameter logistic form for a dose–response curve with a variable slope could be written as $Y = bottom + \left[\frac{top - bottom}{1 + 10^{(\log IC_{50} - x) * h}} \right]$, where Y is the normalized cell survival, x is the log of concentration, top denotes the highest fluorescence intensity, $bottom$ denotes the lowest fluorescence intensity, $LogIC_{50}$ (inhibitory concentration) is the x value

when the response is halfway between bottom and top, and h is the Hill slope of the curve. The curve is shallower when $h < 1$, and steeper when $h > 1$.

The uncertainty of the analysis is determined and quantified using error bars on the dose–response curve. For each concentration, one image from the middle of the well is used to quantify the intensity. For the control well, the average of the four intensities is taken. In the remaining wells containing the toxicant, the intensity of each image is normalized against the average of the control well. The overall live cell percentage is found from the average of these normalized percentages. The error in the measurement is represented as the standard deviation of the four normalized values.

2.6. AFM Analysis

An MFP-3D-Bio atomic force microscope (AFM; Oxford Instruments, Santa Barbara, CA, USA) mounted on an inverted fluorescence microscope (Nikon Eclipse Ti; Melville, NY, USA) was used to measure the changes in biophysical and biomechanical characteristics of ReNcells upon exposure to these compounds. The tip-less cantilevers (Arrow™ TL1, Nanoworld, nominal spring constant: 0.03 N/m) were modified by attaching a 5- μm polystyrene bead using epoxy. The actual spring constant of the beaded tip was obtained using thermal calibration in a dish containing only a culture medium. Cells were cultured (5000 cells/dish) in laminin-coated, AFM-specific, 50 mm Petri dishes for 24 h, and exposed to each compound for 36 h at two specific concentrations: IC_{50} and $\text{IC}_{50}/2$. The IC_{50} values were obtained from the dose–response curves fitted to cell viability assay results. Control cultures did not receive the compounds but received vehicle DMSO or acetone at similar concentrations. Cells were maintained at 37 °C using a BioHeater (Oxford Instruments) and multiple cells ($37 \leq n \leq 101$) were randomly selected from each condition using an optical microscope (Nikon Eclipse Ti; Melville, NY, USA; 20 \times objective). The force-indentation curves obtained at the approach/retraction velocity of 5 $\mu\text{m}/\text{s}$ were analyzed using proprietary Igor Pro 6.37 software (WaveMetrics, Inc. Portland, OR, USA), and the curves were fitted to a Hertz contact model to measure the Young's modulus (E_Y) [31]. The tether forces (F_T) were obtained from the series of force steps in the retraction curves with the threshold set at 30 pN. The apparent membrane tension (T_M) needed to deform a membrane was calculated from F_T using $T_M \cong F_T^2/8\pi^2k_B$, where k_B is the bending stiffness (0.1–0.3 pN. μm) [32–34]. Finally, the tether radius (R_T) that represents the connection between the plasma membrane and cytoskeleton was obtained from F_T as $R_T \cong 2\pi k_B/F_T$ [31].

2.7. Wound Healing Assay

The potential changes in cell migration ability in the presence of these compounds were evaluated using a CytoSelect™ Wound Healing Assay kit (Cell Biolabs, Inc., San Diego, CA, USA). This assay works on the wound healing principle with defined rectangular wound fields (0.9 mm gap) created in confluent cell monolayers using treated inserts. The confluent cell layers in 24-well plates ($n = 4$ wells/concentration/compound) were exposed to either $\text{IC}_{50}/2$ or $\text{IC}_{50}/4$ concentrations of the six individual compounds for 24 h. After the inserts were removed, cell migration and wound closure over 48 h were captured at regular intervals by imaging with a Samsung automated S+ scanner. The images were analyzed using NIH ImageJ (Bethesda, MD, USA) and the percentage reduction in wound area was quantified as per protocols described elsewhere [35,36]. Control cultures did not receive the compounds, whereas cell layers exposed to IC_{50} concentrations did not show noticeable movement.

2.8. Statistical Analysis

Cell viability, DNA content, and cell migration assays were repeated three independent times. The results were analyzed and plotted using GraphPad Prism software and expressed as mean \pm standard error. Comparison between groups was performed by

the non-parametric, Bonferroni-corrected, Mann–Whitney U test. Statistically significant differences between groups were indicated by * for $p < 0.05$.

3. Results and Discussion

3.1. Cell Survival and IC_{50} Values

ReNcells were exposed to six different pesticides, each at ten different concentrations (10 pM to 10 mM). The resulting image intensities were normalized to that from the control wells and a dose–response curve was created to determine the IC_{50} values. Figures 1 and 2 show the representative immunofluorescence images of culture wells after 24 h exposure to various compounds, and stained with calcein AM and Hoechst, respectively. The respective dose–response curves calculated from these cultures are also shown in these figures. When cells were exposed to 4-AP, a large drop in cell survival was noted between 100 μ M and 1 mM concentrations, with IC_{50} around 172 μ M. A similar trend was noted from the Hoechst-stained wells (DNA content) as well ($IC_{50} = 189 \mu$ M). Pyriproxyfen appears to be more toxic than all the compounds tested ($IC_{50} = 8.8 \mu$ M). The effect of the compound was noted at as low as 10 nM, with a large drop in cell density occurring between 10 nM and 100 nM. The number of live cells gradually decreased to 10 mM. Hoechst staining also showed a parallel trend ($IC_{50} = 4.1 \mu$ M). Exposure to temephos showed results similar to pyriproxyfen. The effect of the toxicant is evident even at 1 nM, with a gradual decrease in cell density with increasing concentration ($IC_{50} = 12 \mu$ M).

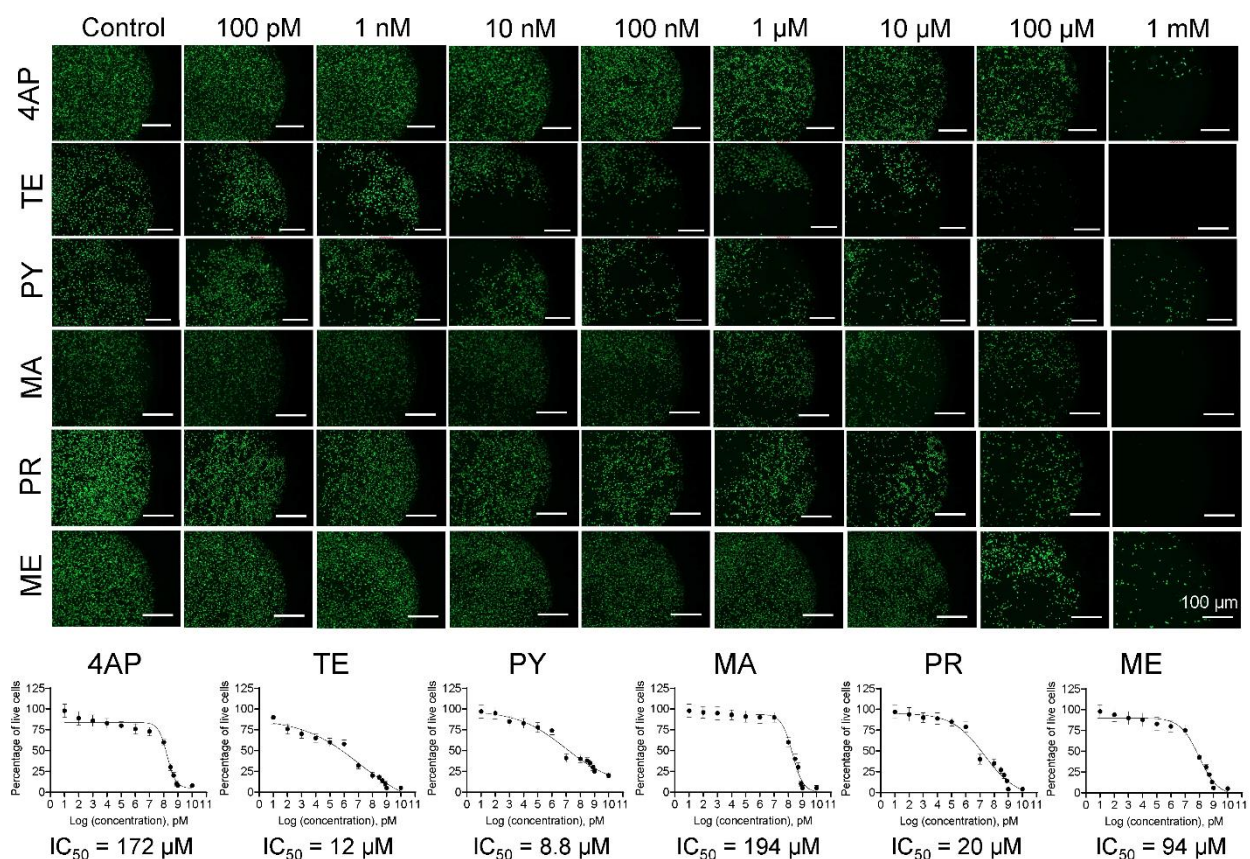


Figure 1. Cell survival assessed using calcein AM staining. Representative immunofluorescence images of ReNcell cultures after 24 h exposure to various compounds and stained with calcein AM. Compound-free cultures served as controls. Scale bar: 100 μ m. Green dots indicate live cells in each image. 4AP—4-Aminopyridine; TE—temephos, PY—pyriproxyfen; MA—malathion; PR—prallethrin; ME—methoprene. The dose–response curves were calculated for ReNcells exposed to various concentrations of each compound for 24 h and stained with calcein AM. The IC_{50} values were obtained from these curves ($R^2 > 0.97$ in all the cases).

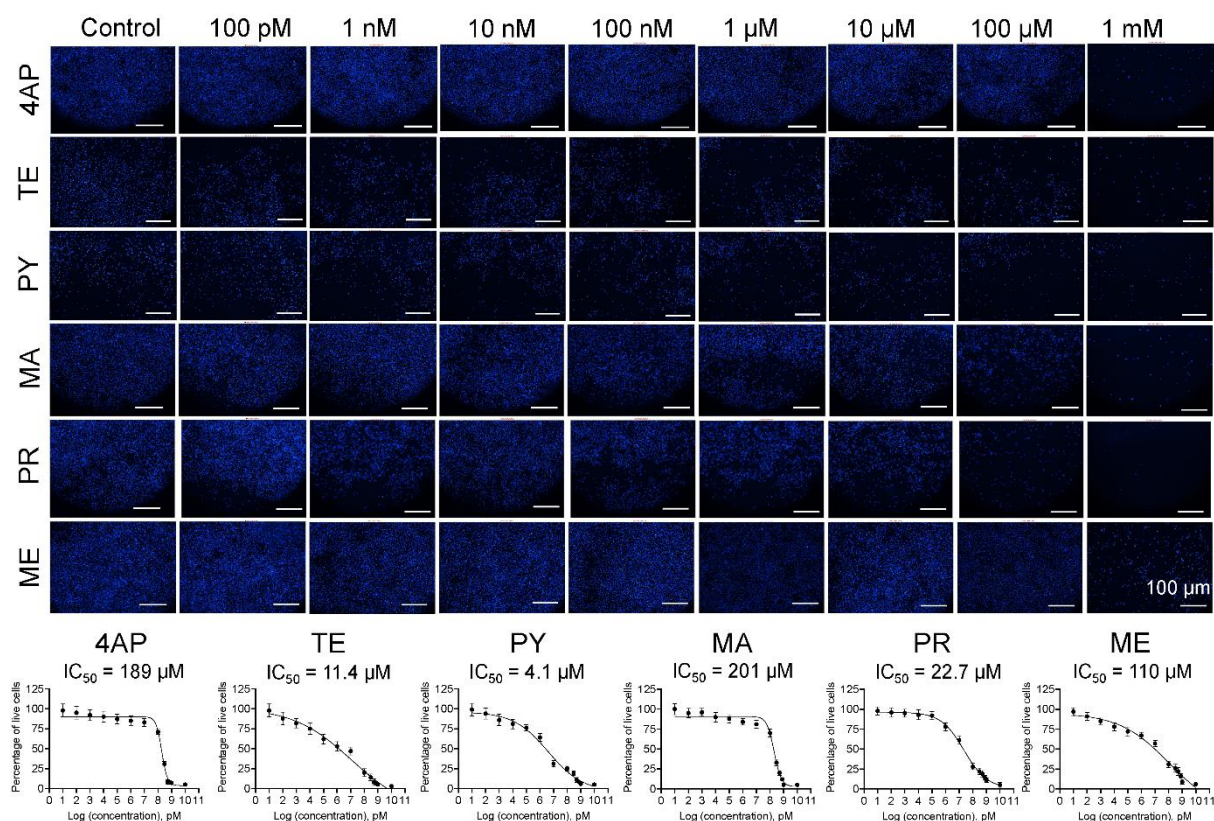


Figure 2. DNA damage assessed using Hoechst staining. Representative immunofluorescence images of ReNcell cultures after 24 h exposure to various compounds and stained with Hoechst. Compound-free cultures served as controls. Scale bar: 100 μm . Blue dots indicate live cells in each image. 4AP—4-Aminopyridine; TE—temephos; PY—pyriproxyfen; MA—malathion; PR—prallethrin; ME—methoprene. The dose–response curves were calculated for ReNcells exposed to various concentrations of each compound for 24 h and stained with Hoechst ($R^2 > 0.98$ in all the cases).

Exposure to malathion showed a trend similar to that of 4-AP, with the compound inducing more impact on live cells starting around 10 μM . A large drop in cell survival occurred above 100 μM concentration, with the IC_{50} value calculated at 194 μM . Results from Hoechst staining closely resembled those of the viability assay ($\text{IC}_{50} = 201 \mu\text{M}$). When exposed to methoprene, cell survival dramatically reduced between 10 μM and 100 μM , with another significant drop at 1 mM, indicating that methoprene ($\text{IC}_{50} = 94 \mu\text{M}$) could be slightly more toxic than 4-AP. Cultures exposed to methoprene and stained with Hoechst showed similar trends ($\text{IC}_{50} = 110 \mu\text{M}$). Prallethrin appeared to be more toxic than both 4-AP and methoprene. The toxicant effect could be seen even at 100 nM. A larger drop in the number of living cells occurred between 10 μM and 100 μM and between 100 μM and 1 mM, with the IC_{50} calculated at 20 μM . Hoechst staining showed trends similar to the viability assay ($\text{IC}_{50} = 22.7 \mu\text{M}$). In 2D cultures, dead cells could detach from the plate upon exposure to toxicants and are washed away during the staining steps.

From the IC_{50} values, it could be seen that the impact of these compounds ranged from relatively very toxic to mildly toxic on fetal NPCs. Figure 3 shows a comparison of the IC_{50} values for each compound. The order of toxicity from the least to the greatest is as follows: malathion < 4-AP < methoprene < prallethrin < temephos < pyriproxyfen. The IC_{50} values we obtained were compared to those reported in a previous study using the ReNcell NPC cell line and 3D cultures but with different compounds [37]. Among these compounds, paraquat is the only known herbicide, and its reported IC_{50} value of 57 μM is within the range of the six compounds we tested here. The limited data that exist in the literature suggests that the IC_{50} values of malathion in rat fetal lung fibroblasts, human HepG2 liver

cells, and mouse kidney cells are 60 μM , 99.4 μM , and 71.1 μM , respectively [38–41], similar in magnitude to that we measured.

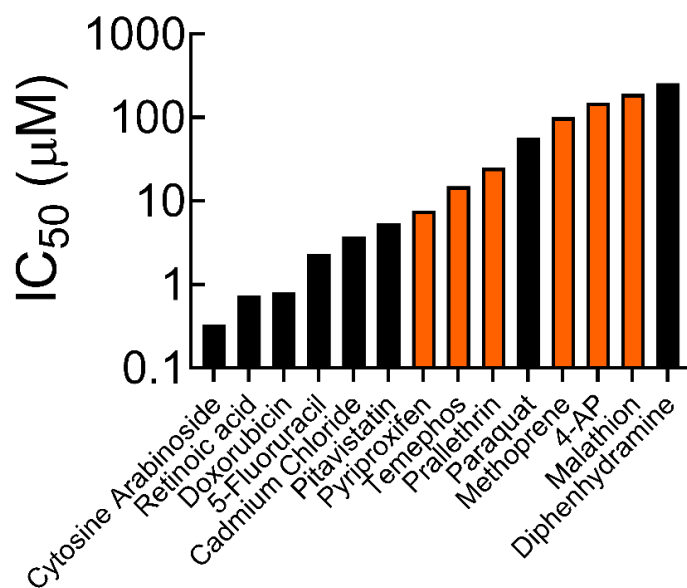


Figure 3. Compound-dependent IC₅₀ values of human fetal NPCs. The IC₅₀ values for compounds in this study were compared to those obtained from a prior study with ReNcells [37]. The orange bars represent compounds tested in this study while the black bars represent those tested in the previous study.

3.2. Cell Mechanics

The biomechanical characterization of cells was done after they were exposed to each compound for 36 h. Our previous studies have shown no significant time-dependent biomechanical changes in control cultures over the 36 h of culture [31]. The average E_Y of cells in control cultures was 5.1 ± 0.19 kPa (Figure 4), similar to what we reported in our previous study on these cells [31]. The average E_Y of cells exposed to IC₅₀/2 concentrations of various pesticide compounds were as follows: PY (1.556 ± 0.128 kPa), PR (2.347 ± 0.094 kPa), TE (2.14 ± 0.165 kPa), ME (2.606 ± 0.036 kPa), 4-AP (2.835 ± 0.056 kPa), and MA (3.213 ± 0.033 kPa). On the other hand, the average E_Y of cells exposed to IC₅₀ concentrations of these pesticide compounds were as follows: PY (1.067 ± 0.13 kPa), PR (1.217 ± 0.12 kPa), TE (1.32 ± 0.032 kPa), ME (1.43 ± 0.078 kPa), AP (1.262 ± 0.022 kPa), and MA (1.483 ± 0.045 kPa). It could be seen that ReNcells in control cultures were significantly stiffer than in those exposed to all six compounds at both the concentrations tested ($p < 0.05$ in all the cases). Additionally, for each compound, the average E_Y of cells exposed to IC₅₀ dose was significantly lower than that of the cells exposed to IC₅₀/2 dose ($p < 0.05$ in all the cases). In summary, the E_Y of fetal NPCs exposed to IC₅₀/2 doses of these compounds was lowered by 38–69%, while that of those exposed to IC₅₀ doses was reduced by 71–80%, attesting to the significant impact of these compounds. The statistical significance in the inter-group differences between E_Y values (Supplementary Table S1) suggests that malathion had the most detrimental impact on these cells compared to others at both IC₅₀ and IC₅₀/2 doses, in agreement with the IC₅₀ value (Figure 1) it exhibited compared to other compounds.

In a recent study [31], we reported that rotenone (insecticide; 0.06–0.27 μM) and chlorpyrifos (organophosphate; 2.5–9.8 μM) significantly reduced the E_Y of ReNcells, as a function of increasing concentration and exposure duration (4–36 h). The IC₅₀ values of these two compounds—0.27 μM and 9.9 μM , respectively—were lower than most of the compounds tested in the current study, indicating their propensity for toxicity even at low concentrations. The average E_Y ranged between 0.6–2.3 kPa after 36 h of exposure (concentration-dependent), which is slightly less ($p < 0.05$) than the E_Y ranges noted for the six compounds explored in this study.

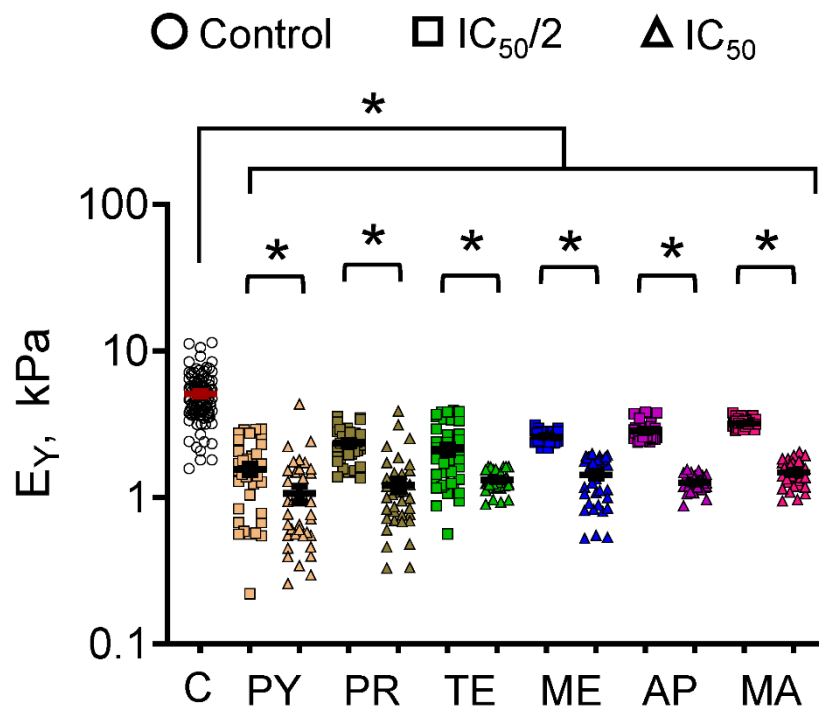


Figure 4. Changes in Young's modulus of human fetal NPCs. The Young's modulus (E_Y) of the ReN-cells was quantified from the force–displacement curves obtained at IC_{50} and $IC_{50}/2$ concentrations of various compounds after 36 h exposure. Multiple cells ($37 \leq n \leq 101$) were selected for each culture condition, and the individual E_Y values as well as the average \pm standard error were plotted. Control cultures (denoted by C) received no compounds. Significant differences between the control cultures and compound-receiving cultures were noted. Additionally, E_Y values were dose-dependent for each compound; i.e., E_Y values for cells receiving IC_{50} dose were significantly lower than those receiving $IC_{50}/2$ dose. * indicates $p < 0.05$. Abbreviations (symbol colors): AP—4-Aminopyridine (magenta); TE—temephos (green); PY—pyriproxyfen (buff); MA—malathion (crimson); PR—prallethrin (olive); ME—methoprene (deep blue).

The trends in tether forces (F_T) and membrane tension (T_M) reflect those in E_Y (Figure 5). The average tether force measured in control cells was 341 ± 4.58 pN. At $IC_{50}/2$ dosage exposure, the tether forces ranged between 135.8 pN to 215.3 pN for the six compounds tested, a 37–60% drop compared to controls ($p < 0.05$ vs. control, for all the compounds). Similarly, at IC_{50} dosages, the average F_T values ranged between 110.3 pN to 174.7 pN for these six compounds, a 49–68% reduction compared to controls ($p < 0.05$ vs. control, $p < 0.05$ for IC_{50} vs. $IC_{50}/2$, for all the compounds). The average membrane tension in control cells in the absence of exogenous compounds was 14.9 ± 0.39 nN/ μ m. Exposure to respective IC_{50} concentrations of the six compounds led to a significant drop, i.e., to 1.63–3.92 nN/ μ m range in T_M values ($p < 0.05$ vs. control, for all the compounds), while exposure to $IC_{50}/2$ concentrations reduced T_M to 2.43–5.91 nN/ μ m range ($p < 0.05$ vs. control, $p < 0.05$ for IC_{50} vs. $IC_{50}/2$, for all the compounds). Finally, the radius of curvature (R_T), which is inversely related to F_T , was significantly higher ($p < 0.05$) in all the test cases compared to controls (1.86 ± 0.025 nm). The range for R_T was 3.65–6.03 nm in cultures receiving IC_{50} dosages ($p < 0.05$ vs. controls, for all the compounds), while it was 2.94–4.77 nm in cultures exposed to $IC_{50}/2$ dosages ($p < 0.05$ vs. controls, $p < 0.05$ for IC_{50} vs. $IC_{50}/2$, for all the compounds).

In general, there is a paucity of literature on the biomechanical characterization of mammalian cells when they are exposed to toxicants. The F_T , T_M and R_T values in control cells were similar to those we reported earlier for ReNcells cultured under similar conditions [31]. After 36 h exposure, the F_T values ranged between 60–190 pN, while the T_M values ranged between 0.4–4.8 nN/ μ m in the presence of rotenone or chlorpyrifos

(concentrations $\leq IC_{50}$), which were significantly lower than that in control cultures at similar time points. These values are within the bounds of F_T and T_M values we observed for the six compounds tested in the current study. Collectively, our results show how toxicant exposure significantly affects E_Y and F_T of ReNcells compared to untreated cells, and that such compromise in E_Y appears to be directly correlated to the IC_{50} values of the toxicants they are exposed to.

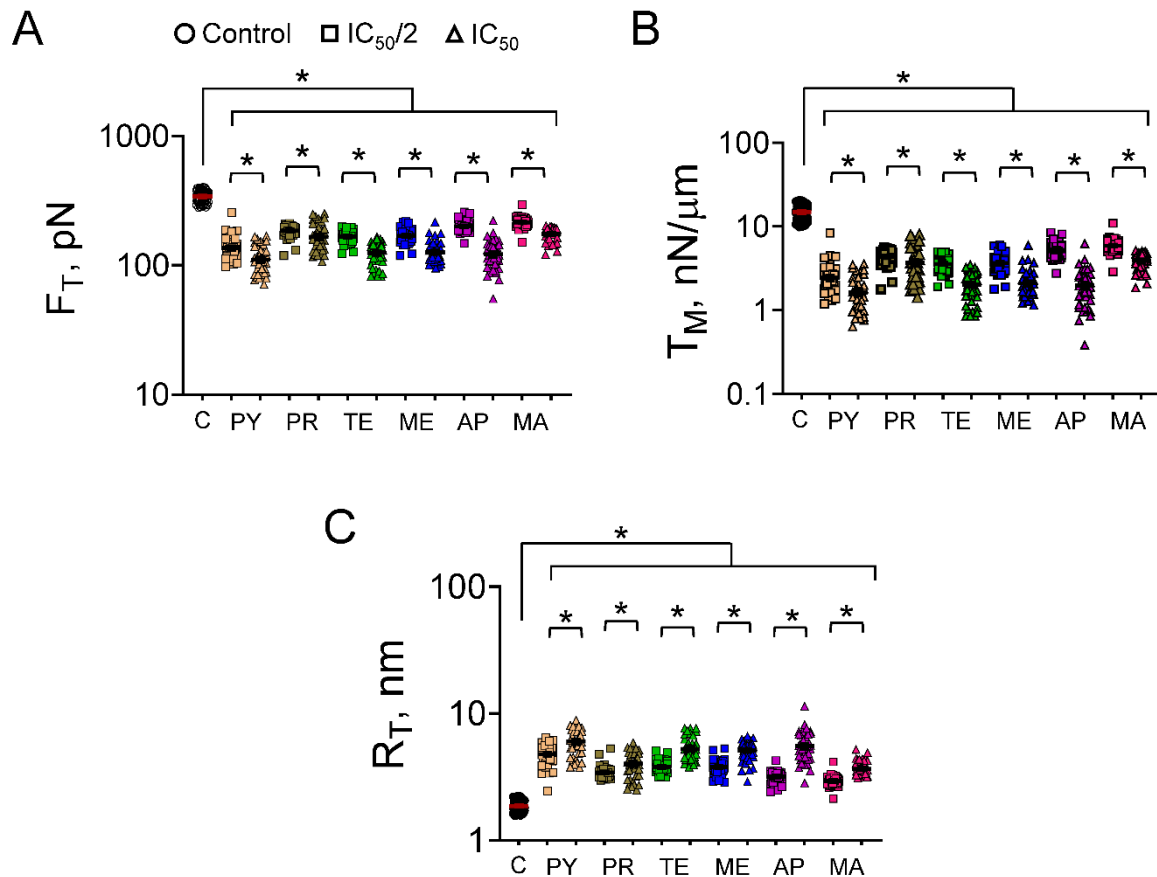


Figure 5. Changes in biomechanical characteristics of ReNcells. (A) tether forces (F_T), (B) apparent membrane tension (T_M), and (C) radius of tether (R_T) were quantified from the force–displacement curves obtained at IC_{50} and $IC_{50}/2$ concentrations of various compounds after 36 h exposure. Multiple cells ($41 \leq n \leq 115$) were selected for each culture condition, and the individual values as well as the average \pm standard error were plotted. Control cultures (denoted by (C)) received no compounds. Significant differences between controls and compound-receiving cultures were noted. Additionally, F_T , T_M , and R_T values were dose-dependent for each compound. * indicates $p < 0.05$. AP—4-Aminopyridine (majenta); TE—temephos (green); PY—pyriproxyfen (buff); MA—malathion (crimson); PR—prallethrin (olive); ME—methoprene (deep blue).

It could be noted from Figure 4 that the variance of E_Y measurements in cells exposed to PY, PR, and TE is higher than the E_Y in cells exposed to ME, 4AP, and MA. In general, biomechanics data tend to have large variances as the sample sizes tend to be large to account for natural variations and stochasticity in the biological processes. We believe that the outliers in the E_Y data might be a normal part of the data distribution, where some cells were more affected than others. Incidentally, quantitative data from Figures 1 and 2 suggest that the IC_{50} values of 4AP, MA, and ME are significantly higher (an order of magnitude) than the IC_{50} values of TE, PR, and PY. This suggests that (i) the internal organelles (nucleus, mitochondria, cell membrane, etc.) of neural stem cells are likely more susceptible to TE, PY, and PR at the IC_{50} and $IC_{50}/2$ concentrations, and (ii) the sub-cellular mechanisms by which these three compounds affect neural stem cells might be different from that by 4AP, MA, and ME.

We have previously shown that mitochondrial membrane potential impairment was the most sensitive mechanism of neurotoxicity in human fetal neural stem cells that were exposed to rotenone, N-arachidonylethanolamine (AEA), and chlorpyrifos, whereas compromise in plasma membrane integrity was the most sensitive mechanism of digoxin impact [31]. We hypothesize that the integrity of bilipid layers or clusters of transmembrane proteins within the bilipid layers was compromised in these cells upon exposure to PY, PR, and TE, leading to high variance in the observed E_{γ} data, i.e., region-specific heterogeneity in the cell surface stiffness. The sub-cellular mechanisms by which these six compounds affect the human fetal neural stem cells will be elucidated in our future studies.

We have shown earlier that in the presence of pesticides, such as rotenone and chlorpyrifos, mitochondrial impairment appears to be the dominant mechanism by which ReNcell health and phenotype were affected [31]. Significant compromise in cell morphology (reduced cell area and spreading) and cytoskeletal actin consolidation at the cell periphery was evident in such cultures, although no changes in SOX2 (stemness marker) expression were noted in the surviving cells. Similar outcomes could be expected even in the presence of the six compounds tested in the current study.

Organophosphates in general have been known to induce both acute and chronic neurotoxicity and lead to cell death by necrosis, apoptosis, or acetylcholinesterase activity (AChE) inhibition. Studies have shown that in numerous species, including humans, malathion induces cell cytotoxicity, intracellular reactive oxygen species, DNA damage, lipid peroxidation, oxidative stress, neuroinflammation, as well as cell cycle arrest, and activates mitochondrial apoptotic pathways [42,43]. In 3D brain-on-a-chip cultures of neurons and astrocytes derived from human induced pluripotent stem cells, exposure to various concentrations of malathion inhibited AChE activity and compromised cell viability, which was rescued by the addition of butyrylcholinesterase [44]. Prenatal exposure to non-AChE inhibiting doses of malathion induced developmental neurotoxicity (memory impairment and spatial learning deficits) in guinea pigs, highlighting the significant impact it has on developmental neurotoxicity [45]. Interestingly, OP mixtures (malathion and chlorpyrifos) exhibited synergistic toxic effects and appeared lethal at concentrations that were sublethal in standalone conditions [46,47]. The developmental neurotoxicity of some of these compounds could be second-handed in nature. For instance, when pyriproxyfen was used as a larvicide to control mosquitoes responsible for Zika virus transmission, its impact on neurodevelopmental disorders in humans outweighed that of the virus transmission itself [48].

3.3. Cell Migration

A wound healing assay is commonly used to quantitatively assess cell migration patterns in monolayer cultures. Though not truly indicative of cellular behavior in vivo, such an assay nevertheless yields valuable data on cell population response to various exogenous compounds and their dosages, fit for screening purposes. Prior in vitro studies on ReNcell migration, conducted in the presence of cocultures (glioblastoma cells and astrocytes) or conditioned media revealed the mechanisms underlying such interactions in such microenvironments [49–51]. At IC_{50} concentrations, ReNcell movement was barely noted in our study, as some cells were dead and detached from the surface over the 48 h study, while those that survived barely moved. Therefore, lower concentrations ($IC_{50}/2$ and $IC_{50}/4$) were tested for their influence on ReNcell migration.

Sheet-like collective cell migration, typical in epithelial cells, was not evident in these cultures. Cell migration was the fastest in control cultures, covering most of the scratch area within the first 12 h after insert removal (Figure 6). When exposed to these six compounds, cell migration slowed at both concentrations compared to controls, with the lowest in cultures exposed to PY, TE, and PR. Statistically significant differences exist between (i) $IC_{50}/2$ and $IC_{50}/4$ concentrations at all time points in cultures exposed to PY; (ii) between $IC_{50}/2$ and $IC_{50}/4$ concentrations only at the 6 h time point in cultures exposed to MA, and only at the 48 h time point in cultures exposed to 4-AP; and (iii) no

significant differences exist between these two concentrations in cultures exposed to PR, ME, and controls. This can be justified as these three compounds exhibited higher levels of toxicity as evident from their IC_{50} values. The cell migration under exposure to these three compounds agreed with their cell survival and biomechanics results, as discussed earlier. We hypothesize that alterations in the cell membrane, bilipid layer composition, and intracellular cytoskeletal protein machinery (e.g., actin filaments) in the cells exposed to various doses of toxicants might be the underlying cause of these observed patterns in cell migration. The lack of significant differences between the two concentrations in some cases suggests that $IC_{50}/4$ dosage is sufficient to induce significant changes in cell mobilization machinery, whereas higher concentrations ($\geq IC_{50}$) would lead to cell death via apoptosis or necrosis pathways. This hypothesis will be tested in our future studies.

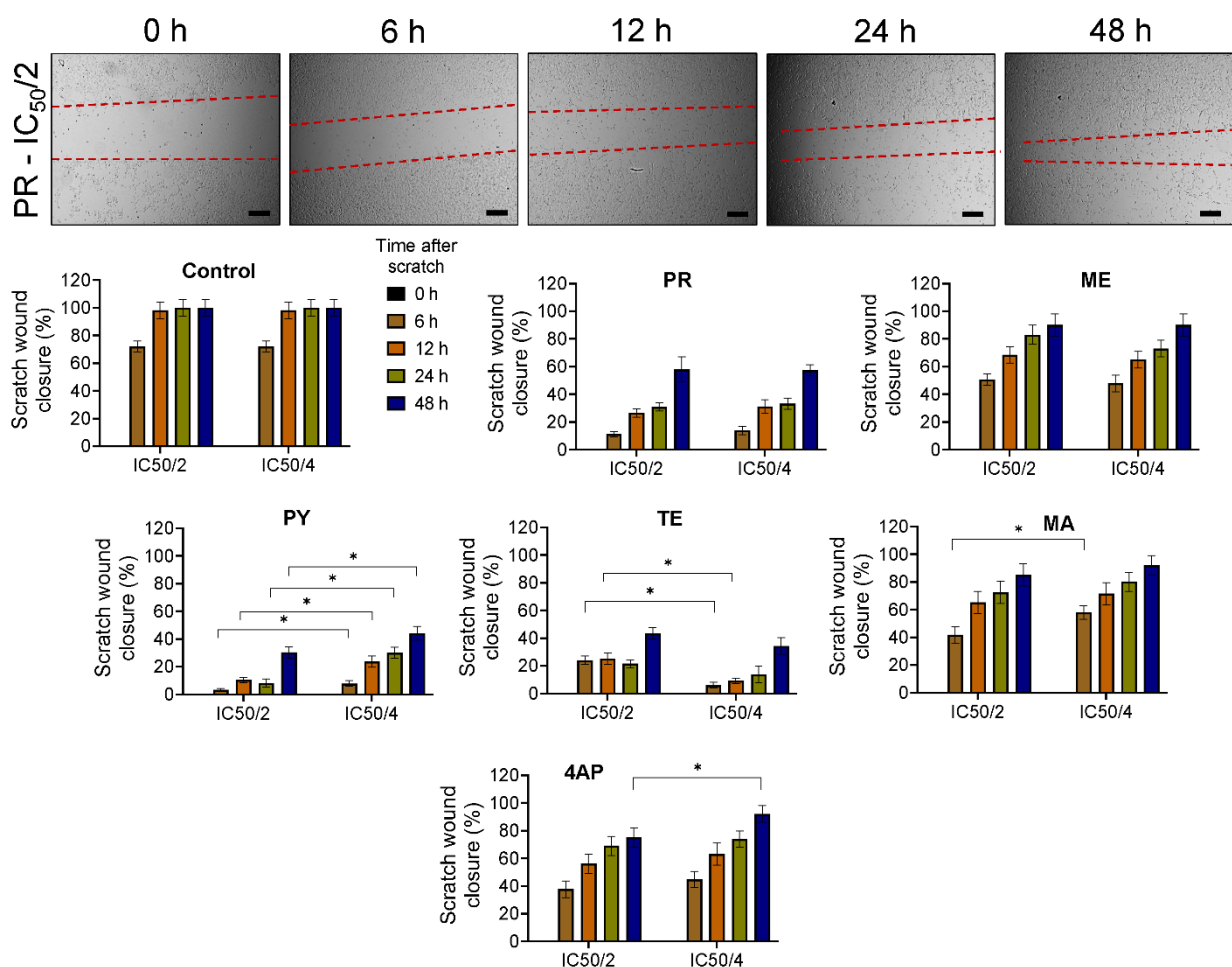


Figure 6. Cell migration assay. ReNcell migration patterns over 48 h were assessed via a scratch wound healing assay, in cultures receiving various dosages ($IC_{50}/2$, $IC_{50}/4$) of the six compounds. Representative phase-contrast images of the scratch closure at various time points were shown in cultures receiving prallethrin at $IC_{50}/2$ dosage. The red dotted lines in the images trace the edge of the cell migration front. The reduction in the scratch area was quantified under various conditions (compounds, dosages) and plotted for comparison. Scale bar: 500 μ m. * indicates $p < 0.05$.

There is a paucity of literature on ReNcell migration in vitro under exposure to insecticides or pesticides. However, others have reported a similar reduction in migration speed and the number of cells migrating when exposed to pesticide or insecticide compounds in vitro. For instance, human NT2 cells had significantly reduced migration in vitro in a concentration-dependent manner, when exposed to rotenone or fipronil, even at nanomolar concentration levels [52]. Rotenone exposure also inhibited the migration of neural stem cells derived from the rat E16 mesencephalon in a dose-dependent manner [53]. The

migration and tube formation capabilities of human umbilical vein endothelial cells were severely repressed in a dose-dependent manner when exposed to permethrin—a synthetic pyrethroid insecticide, facilitated possibly by elevated reactive oxygen species production [54]. Taken together, the biomechanical changes induced by exposure to these pesticide compounds might have contributed to the compromise in cell migration patterns in vitro.

4. Conclusions

In this study, we assessed the influence of the active ingredients of six pesticides on human fetal NPC phenotype, survival, and changes in biomechanical (Young's modulus, tether force, membrane tension, and tether radius) characteristics in vitro. Based on their IC_{50} values, which span over an order of magnitude, the order of toxicity is malathion < 4-AP < methoprene < prallethrin < temephos < pyriproxyfen. When NPCs were exposed to these six compounds at IC_{50} or $IC_{50}/2$ concentrations in vitro, a significant compromise in the Young's modulus, tether forces, and apparent membrane tension was noted (AFM analysis), with higher dosages being more impactful. The NPC migration was also curtailed in the presence of these compounds, even at $IC_{50}/4$ dosage, possibly due to the changes in their biomechanical characteristics. Our future studies will explore the sub-cellular mechanisms by which each of these compounds influences changes in the NPC phenotype and biomechanical changes. Our study provides evidence of the significant role of *mechanotoxicology* in the phenotype and characteristics of human fetal neural progenitor cells during development stages.

Supplementary Materials: The following supporting information can be downloaded at: <https://www.mdpi.com/article/10.3390/biophysica3020023/s1>, Table S1: Statistical significance (p -value < 0.05) between E_Y values of cells exposed to various culture conditions (compound and dosage) was calculated using Student's t -test. The values highlighted in red indicate no difference ($p > 0.05$) between the compared groups.

Author Contributions: Conceptualization: C.R.K.; methodology, validation, formal analysis, investigation: M.C.S., J.V., S.M.A. and N.A.; writing—original draft preparation: M.C.S. and C.R.K.; writing—review and editing, visualization, resources, supervision, project administration, funding acquisition: C.R.K. All authors have read and agreed to the published version of the manuscript.

Funding: This work was partially supported by the National Institutes of Health (NIEHS R01ES025779) and the National Science Foundation (CBET Award # 1337859) to CK; the Jack, Joseph, and Morton Mandel Honors College at Cleveland State University to Marissa Sarsfield; the National Institutes of Health's Bridges to Success in the Sciences (NIGMS 5R25GM049010-15) funding to Jennifer Vasu and Sabreen Abuoun.

Data Availability Statement: Data would be made available upon reasonable request.

Acknowledgments: Marissa Sarsfield, Jennifer Vasu, and Sabreen Abuoun were undergraduates when they performed this work. They acknowledge the technical assistance and training from Gautam Mahajan and Pranav Joshi in setting up the AFM measurements and cell migration assays, respectively.

Conflicts of Interest: The authors declare no conflict of interest.

References

1. Zhang, W. Global pesticide use: Profile, trend, cost/benefit and more. *Proc. Int. Acad. Ecol. Environ. Sci.* **2018**, *8*, 1–27.
2. Food and Agriculture Organization. *FAOSTAT: Database Collection of the Food and Agriculture Organization of the United Nations*; FAO: Rome, Italy, 2019.
3. Sharma, A.; Kumar, V.; Shahzad, B.; Tanveer, M.; Sidhu, G.P.; Handa, N.; Kohli, S.K.; Yadav, P.; Bali, A.S.; Parihar, R.D.; et al. Worldwide pesticide usage and its impacts on ecosystem. *SN Appl. Sci.* **2019**, *1*, 1446. [[CrossRef](#)]
4. Boedeker, W.; Watts, M.; Clausing, P.; Marquez, E. The global distribution of acute unintentional pesticide poisoning: Estimations based on a systematic review. *BMC Public Health* **2020**, *20*, 1875. [[CrossRef](#)]
5. Tang, F.H.; Lenzen, M.; McBratney, A.; Maggi, F. Risk of pesticide pollution at the global scale. *Nat. Geosci.* **2021**, *14*, 206–210. [[CrossRef](#)]
6. Mnif, W.; Hassine, A.I.H.; Bouaziz, A.; Bartegi, A.; Thomas, O.; Roig, B. Effect of Endocrine Disruptor Pesticides: A Review. *Int. J. Environ. Res. Public Health* **2011**, *8*, 2265–2303. [[CrossRef](#)]

7. Gilden, R.C.; Huffling, K.; Sattler, B. Pesticides and Health Risks. *J. Obstet. Gynecol. Neonatal Nurs.* **2010**, *39*, 103–110. [[CrossRef](#)]
8. Mehrpour, O.; Karrari, P.; Zamani, N.; Tsatsakis, A.M.; Abdollahi, M. Occupational exposure to pesticides and consequences on male semen and fertility: A review. *Toxicol. Lett.* **2014**, *230*, 146–156. [[CrossRef](#)]
9. Kallioraab, C.; Mamoulakis, C.; Vasilopoulos, E.; Stamatiades, G.A.; Kalafati, L.; Barouni, R.; Karakousi, T.; Abdollahi, M.; Tsatsakis, A. Association of pesticide exposure with human congenital abnormalities. *Toxicol. Appl. Pharmacol.* **2018**, *346*, 58–75. [[CrossRef](#)] [[PubMed](#)]
10. Alavanja, M.C.R. Pesticides Use and Exposure Extensive Worldwide. *Rev. Environ. Health* **2009**, *24*, 303–309. [[CrossRef](#)] [[PubMed](#)]
11. Kim, K.-H.; Kabir, E.; Jahan, S.A. Exposure to Pesticides and The Associated Human Health Effects. *Sci. Total Environ.* **2017**, *575*, 525–535. [[CrossRef](#)]
12. Tudi, M.; Li, H.; Li, H.; Wang, L.; Lyu, J.; Yang, L.; Tong, S.; Yu, Q.J.; Ruan, H.D.; Atabila, A.; et al. Exposure Routes and Health Risks Associated with Pesticide Application. *Toxics* **2022**, *10*, 335. [[CrossRef](#)]
13. Aktar, M.W.; Sengupta, D.; Chowdhury, A. Impact of Pesticides Use in Agriculture: Their Benefits and Hazards. *Interdiscip. Toxicol.* **2009**, *2*, 1–12. [[CrossRef](#)]
14. Carvalho, F.P. Pesticides, Environment, and Food Safety. *Food Energy Secur.* **2017**, *6*, 48–60. [[CrossRef](#)]
15. Monteiro, J.P.; Jurado, A.S. Methoprene. In *Encyclopedia of Toxicology*, 3rd ed.; Academic Press/Elsevier: London, UK, 2014; pp. 246–249.
16. Ramaseshadri, P.; Farkaš, R.; Palli, S.R. Recent Progress in Juvenile Hormone Analogs (JHA) Research. *Adv. Insect Physiol.* **2012**, *43*, 353–436.
17. Devillers, J. Fate of Pyriproxyfen in Soils and Plants. *Toxics* **2020**, *8*, 20. [[CrossRef](#)]
18. Kumar, S.S.; Ghosh, P.; Malyan, S.K.; Sharma, J. A comprehensive review on enzymatic degradation of the organophosphate pesticide malathion in the environment. *J. Environ. Sci. Health* **2019**, *37*, 288–329. [[CrossRef](#)] [[PubMed](#)]
19. Casida, J.E.; Quistad, G.B. Organophosphate toxicology: Safety aspects of nonacetylcholinesterase secondary targets. *Chem. Res. Toxicol.* **2004**, *17*, 983–998. [[CrossRef](#)] [[PubMed](#)]
20. Katsuda, Y. Progress and Future of Pyrethroids. In *Pyrethroids. Topics in Current Chemistry*; Matsuo, N., Mori, T., Eds.; Springer: Berlin/Heidelberg, Germany, 2011; Volume 314.
21. Georgiadis, N.; Tsarouhas, K.; Tsitsimpikou, C.; Vardavas, A.; Rezaee, R.; Germanakis, I.; Tsatsakis, A.; Stagos, D.; Kouretas, D. Pesticides and cardiotoxicity. Where do we stand? *Toxicol. Appl. Pharmacol.* **2018**, *353*, 1–14. [[CrossRef](#)]
22. Schafer, E.W.; Brunton, R.B.; Cunningham, D.J. A summary of the acute toxicity of 4-aminopyridine to birds and mammals. *Toxicol. Appl. Pharmacol.* **1978**, *26*, 532–538. [[CrossRef](#)] [[PubMed](#)]
23. London, L.; Beseler, C.; Bouchard, M.F.; Bellinger, D.C.; Colosio, C.; Grandjean, P.; Harari, R.; Kootbodien, T.; Kromhout, H.; Little, F.; et al. Neurobehavioral and neurodevelopmental effects of pesticide exposures. *Neurotoxicology* **2012**, *33*, 887–896. [[CrossRef](#)]
24. Burns, C.J.; McIntosh, L.J.; Mink, P.J.; Jurek, A.M.; Li, A.A. Pesticide exposure and neurodevelopmental outcomes: Review of the epidemiologic and animal studies. *J. Toxicol. Environ. Health B Crit. Rev.* **2013**, *16*, 127–283. [[CrossRef](#)]
25. Sapbamrer, R.; Hongsihsong, S. Effects of prenatal and postnatal exposure to organophosphate pesticides on child neurodevelopment in different age groups: A systematic review. *Environ. Sci. Pollut. Res. Int.* **2019**, *26*, 18267–18290. [[CrossRef](#)]
26. Muñoz-Quezada, M.T.; Lucero, B.A.; Barr, D.B.; Steenland, K.; Levy, K.; Ryan, P.B.; Iglesias, V.; Alvarado, S.; Concha, C.; Rojas, E.; et al. Neurodevelopmental effects in children associated with exposure to organophosphate pesticides: A systematic review. *Neurotoxicology* **2013**, *39*, 158–168. [[CrossRef](#)] [[PubMed](#)]
27. Sidhu, G.K.; Singh, S.; Kumar, V.; Dhanjal, D.S.; Datta, S.; Singh, J. Toxicity, monitoring and biodegradation of organophosphate pesticides: A review. *Crit. Rev. Environ. Sci. Technol.* **2019**, *49*, 1135–1187. [[CrossRef](#)]
28. Franze, K. The mechanical control of nervous system development. *Development* **2013**, *140*, 3069–3077. [[CrossRef](#)] [[PubMed](#)]
29. Barnes, J.M.; Przybyla, L.; Weaver, V.M. Tissue mechanics regulate brain development, homeostasis and disease. *J. Cell Sci.* **2017**, *130*, 71–82. [[CrossRef](#)]
30. Donato, R.; Miljan, E.A.; Hines, S.J.; Aouabdi, S.; Pollock, K.; Patel, S.; Edwards, F.A.; Sinden, J.D. Differential development of neuronal physiological responsiveness in two human neural stem cell lines. *BMC Neurosci.* **2007**, *8*, 36. [[CrossRef](#)]
31. Mahajan, G.; Lee, M.Y.; Kothapalli, C.R. Biophysical and biomechanical properties of neural progenitor cells as indicators of developmental neurotoxicity. *Arch. Toxicol.* **2019**, *93*, 2979–2992. [[CrossRef](#)]
32. Diz-Munoz, A.; Fletcher, D.A.; Weiner, O.D. Use the force: Membrane tension as an organizer of cell shape and motility. *Trends Cell Biol.* **2013**, *23*, 47–53. [[CrossRef](#)] [[PubMed](#)]
33. Diz-Munoz, A.; Krieg, M.; Bergert, M.; Ibarlucea-Benitez, I.; Muller, D.J.; Paluch, E.; Heisenberg, C.P. Control of directed cell migration in vivo by membrane-to-cortex attachment. *PLoS Biol.* **2010**, *8*, e1000544. [[CrossRef](#)] [[PubMed](#)]
34. Hochmuth, R.M.; Shao, J.Y.; Dai, J.; Sheetz, M.P. Deformation and Flow of Membrane into Tethers Extracted from Neuronal Growth Cones. *Biophys. J.* **1996**, *70*, 358–369. [[CrossRef](#)]
35. Martinotti, S.; Ranzato, E. Scratch Wound Healing Assay. *Methods Mol. Biol.* **2020**, *2109*, 225–229.
36. Suarez-Arnedo, A.; Figueroa, F.T.; Clavijo, C.; Arbeláez, P.; Cruz, J.C.; Muñoz-Camargo, C. An image J plugin for the high throughput image analysis of in vitro scratch wound healing assays. *PLoS ONE* **2020**, *15*, e0232565. [[CrossRef](#)] [[PubMed](#)]
37. Nierode, G.J.; Perea, B.C.; McFarland, S.K.; Pascoal, J.F.; Clark, D.S.; Schaffer, D.V.; Dordick, J.S. High-Throughput Toxicity and Phenotypic Screening of 3D Human Neural Progenitor Cell Cultures on a Microarray Chip Platform. *Stem Cell Rep.* **2016**, *7*, 970–982. [[CrossRef](#)] [[PubMed](#)]

38. Chiba, S.; Ikawa, T.; Takeshita, H.; Kanno, S.; Nagai, T.; Takada, M.; Mukai, T.; Wempe, M.F. Human organic cation transporter 2 (hOCT2): Inhibitor studies using S2-hOCT2 cells. *Toxicology* **2013**, *310*, 98–103. [[CrossRef](#)]
39. Masoud, L.; Vijayasarathy, C.; Fernandez-Cabezudo, M.; Petroianu, G.; Saleh, A.M. Effect of malathion on apoptosis of murine L929 fibroblasts: A possible mechanism for toxicity in low dose exposure. *Toxicology* **2003**, *185*, 89–102. [[CrossRef](#)] [[PubMed](#)]
40. Karami-Mohajeri, S.; Najafi, A.; Behnam, B.; Sadeghi-Meymandi, M.; Kashitarash-Ifahani, Z.; Jafari, E.; Heidari, M.; Mohamadi, N.; Sharififar, F. Protective effect of *Zataria multiflora* Boiss. and its main compound, rosmarinic acid, against malathion induced oxidative stress and apoptosis in HepG2 cells. *J. Environ. Sci. Health B* **2021**, *56*, 297–306. [[CrossRef](#)]
41. Samimi, A.; Last, J.A. Inhibition of lysyl hydroxylase by malathion and malaoxon. *Toxicol. Appl. Pharmacol.* **2001**, *172*, 203–209. [[CrossRef](#)]
42. Elmorsy, E.; Al-Ghafari, A.; Al Doghaither, H.; Salama, M.; Carter, W.G. An Investigation of the Neurotoxic Effects of Malathion, Chlorpyrifos, and Paraquat to Different Brain Regions. *Brain Sci.* **2022**, *12*, 975. [[CrossRef](#)]
43. Shieh, P.; Jan, C.R.; Liang, W.Z. The protective effects of the antioxidant N-acetylcysteine (NAC) against oxidative stress-associated apoptosis evoked by the organophosphorus insecticide malathion in normal human astrocytes. *Toxicology* **2019**, *417*, 1–14. [[CrossRef](#)]
44. Liu, L.; Koo, Y.; Russell, T.; Gay, E.; Li, Y.; Yun, Y. Three-dimensional brain-on-chip model using human iPSC-derived GABAergic neurons and astrocytes: Butyrylcholinesterase post-treatment for acute malathion exposure. *PLoS ONE* **2020**, *15*, e0230335. [[CrossRef](#)]
45. Lumsden, E.W.; McCowan, L.; Pescrille, J.D.; Fawcett, W.P.; Chen, H.; Albuquerque, E.X.; Mamczarz, J.; Pereira, E.F.R. Learning and memory retention deficits in prepubertal guinea pigs prenatally exposed to low levels of the organophosphorus insecticide malathion. *Neurotoxicol. Teratol.* **2020**, *81*, 106914. [[CrossRef](#)] [[PubMed](#)]
46. Pham, B.; Miranda, A.; Allinson, G.; Nugegoda, D. Assessing interactive mixture toxicity of carbamate and organophosphorus insecticides in the yabby (*Cherax destructor*). *Ecotoxicology* **2018**, *27*, 1217–1224. [[CrossRef](#)] [[PubMed](#)]
47. Arora, S.; Balotra, S.; Pandey, G.; Kumar, A. Binary combinations of organophosphorus and synthetic pyrethroids are more potent acetylcholinesterase inhibitors than organophosphorus and carbamate mixtures: An in vitro assessment. *Toxicol. Lett.* **2017**, *268*, 8–16. [[CrossRef](#)]
48. Audouze, K.; Taboureau, O.; Grandjean, P. A systems biology approach to predictive developmental neurotoxicity of a larvicide used in the prevention of Zika virus transmission. *Toxicol. Appl. Pharmacol.* **2018**, *354*, 56–63. [[CrossRef](#)]
49. Díaz-Coránguez, M.; Segovia, J.; López-Ornelas, A.; Puerta-Guardo, H.; Ludert, J.; Chávez, B.; Meraz-Cruz, N.; González-Mariscal, L. Transmigration of Neural Stem Cells across the Blood Brain Barrier Induced by Glioma Cells. *PLoS ONE* **2013**, *8*, e60655. [[CrossRef](#)] [[PubMed](#)]
50. Farrell, K.; Mahajan, G.; Srinivasan, P.; Lee, M.Y.; Kothapalli, C.R. Pediatric glioblastoma cells inhibit neurogenesis and promote astrogenesis, phenotypic transformation and migration of human neural progenitor cells within cocultures. *Exp. Cell Res.* **2018**, *362*, 159–171. [[CrossRef](#)]
51. Li, X.; Liu, X.; Zhao, W.; Wen, X.; Zhang, N. Manipulating neural-stem-cell mobilization and migration in vitro. *Acta Biomater.* **2012**, *8*, 2087–2095. [[CrossRef](#)]
52. Schmitz, A.; Dempewolf, S.; Tan, S.; Bicker, G.; Stern, M. Developmental Neurotoxicity of Fipronil and Rotenone on a Human Neuronal In Vitro Test System. *Neurotox. Res.* **2021**, *39*, 1189–1202. [[CrossRef](#)]
53. Ishido, M.; Suzuki, J. Inhibition by rotenone of mesencephalic neural stem-cell migration in a neurosphere assay in vitro. *Toxicol. In Vitro* **2010**, *24*, 552–557. [[CrossRef](#)]
54. Lee, H.S.; Song, H.J.; Park, Y.; Smolensky, D.; Lee, S.H. Permethrin inhibits tube formation and viability of endothelial cells. *J. Sci. Food Agric.* **2022**, *102*, 4079–4085. [[CrossRef](#)] [[PubMed](#)]

Disclaimer/Publisher’s Note: The statements, opinions and data contained in all publications are solely those of the individual author(s) and contributor(s) and not of MDPI and/or the editor(s). MDPI and/or the editor(s) disclaim responsibility for any injury to people or property resulting from any ideas, methods, instructions or products referred to in the content.